PHYSICAL REVIEW C **89**, 041303(R) (2014)

Shell and shape evolution at $N = 28$: The ^{40}Mg ground state

H. L. Crawford,[1,*] P. Fallon,[1] A. O. Macchiavelli,[1] R. M. Clark,[1] B. A. Brown,[2] J. A. Tostevin,[2,3] D. Bazin,[2] N. Aoi,[4] P. Doornenbal,[4] M. Matsushita,[4] H. Scheit,[4] D. Steppenbeck,[4] S. Takeuchi,[4] H. Baba,[4] C. M. Campbell,[1] M. Cromaz,[1] E. Ideguchi,[5] N. Kobayashi,[6] Y. Kondo,[6] G. Lee,[6] I. Y. Lee,[1] J. Lee,[4] K. Li,[4] S. Michimasa,[5] T. Motobayashi,[4] T. Nakamura,[6] S. Ota,[5] S. Paschalis,[1] M. Petri,[1,†] T. Sako,[5] H. Sakurai,[4] S. Shimoura,[5] M. Takechi,[4] Y. Togano,[4] H. Wang,[4] and K. Yoneda[4]

[1]*Nuclear Science Division, Lawrence Berkeley National Laboratory, Berkeley, California 94720, USA*

[2]*National Superconducting Cyclotron Laboratory, Michigan State University, East Lansing, Michigan 48824, USA*

[3]*Department of Physics, University of Surrey, Guildford, Surrey GU2 7XH, United Kingdom*

[4]*RIKEN Nishina Center, Wako, Saitama 351-0198, Japan*

[5]*Center for Nuclear Study, University of Tokyo, RIKEN Campus, Wako, Saitama 351-0198, Japan*

[6]*Department of Physics, Tokyo Institute of Technology, Meguro, Tokyo 152-8551, Japan*

(Received 20 December 2013; published 30 April 2014)

A measurement of the direct two-proton removal from ^{42}Si has provided the first structural information on the $N = 28$ isotone ^{40}Mg. The value for the inclusive cross section for two-proton removal from ^{42}Si of 40^{+27}_{-17} μb is significantly lower than that predicted by structure calculations using the recent SDPF-MU shell-model effective interaction combined with eikonal reaction theory. This observed discrepancy is consistent with the interpretation that only one of the predicted low-lying 0^+ states in ^{40}Mg is bound. A two-state mixing analysis describing two-proton knockout cross sections along $N = 28$ provides support for the interpretation of a prolate-deformed ^{40}Mg ground state.

DOI: 10.1103/PhysRevC.89.041303 PACS number(s): 25.60.−t, 27.40.+z, 29.38.Db

The study of nuclei far from the line of β stability is one of the most active and challenging areas of current nuclear structure physics. Exotic combinations of protons (Z) and neutrons (N) can significantly affect the underlying shell structure, and for weakly bound nuclei at or near the dripline, the proximity to continuum states may further alter nuclear properties. Benchmarking and constraining theory at the very limits of existence is critical, and one of the most exotic neutron-rich nuclei currently accessible to experiment is ^{40}Mg.

First observed following fragmentation of a ^{48}Ca primary beam at the National Superconducting Cyclotron Laboratory in 2007 (with three events) [1], $^{40}_{12}$Mg$_{28}$ lies at an intersection for nucleon magic numbers and the neutron dripline. It is expected to exhibit [2] the collective and deformed properties characteristic of the $N = 28$ isotones below ^{48}Ca, which is a region of rapidly changing nuclear shapes. Large-scale shell-model calculations predict that ^{40}Mg should be a well-deformed prolate rotor [3]. In addition, the last bound neutron orbital is expected to be the low-l $p_{3/2}$ state, leading to the possibility that weak binding effects could play a role.

Further, deformation along the $Z = 12$ isotopic chain has been of recent experimental interest, with the work of Doornenbal *et al.* [4], in which an extended region of deformation in the Mg isotopes from the quenched $N = 20$ gap out to $N = 26$ is observed, as determined by the ratio of $E(4^+_1)/E(2^+_1)$, and is expected to persist at $N = 28$.

We present here the first experimental structure information on ^{40}Mg following measurement of the inclusive two-proton removal cross section from ^{42}Si and discuss the results as a part of the overall shape evolution along the $N = 28$ isotonic chain. We provide a limit on the number of bound states predicted by theory, and evidence supporting a prolate-deformed ^{40}Mg ground state based on a two-state mixing model.

One- and two-proton knockout reactions from ^{42}Si were carried out at Radioactive Isotope Beam Factory (RIBF), operated by RIKEN Nishina Center and the Center for Nuclear Study, University of Tokyo. A primary beam of ^{48}Ca, at an energy of 345 MeV/nucleon, with an average intensity of approximately 70 pnA, was fragmented in a thick (15-mm) rotating Be production target to produce a cocktail of projectile-like fragments. The secondary beam of interest, ^{42}Si, was selected through the BigRIPS fragment separator [5]. The production rate was ∼0.24 pps/pnA of ^{48}Ca, using the maximum BigRIPS momentum acceptance of 6%. Secondary beam fragments were identified event by event through a combination of energy loss and time-of-flight measurements prior to impinging on the secondary carbon reaction target with thickness 4.02 g/cm^2. The secondary target, used to induce proton knockout, was placed at the focal point immediately upstream of the ZeroDegree spectrometer (ZDS) [6]. Reaction products were uniquely identified in the ZDS.

The upper panel (a) in Fig. 1 shows the particle identification plot for the analyzed incoming secondary beam cocktail, highlighting the incoming ^{42}Si nuclei. The lower panel, Fig. 1(b), shows the particle identification for the nuclei transmitted through the ZDS which were produced following interaction of a ^{42}Si nucleus in the secondary reaction target. A total of five events of ^{40}Mg were observed for 9.65×10^5 incident ^{42}Si nuclei.

The inclusive two proton-knockout cross section from ^{42}Si to ^{40}Mg was measured to be 40^{+27}_{-17} μb at a midtarget energy of 238 MeV/nucleon. This inclusive cross section includes

*Institute of Nuclear and Particle Physics, Department of Physics and Astronomy, Ohio University, Athens, OH 45701, USA.

†Institut für Kernphysik, Technische Universität Darmstadt, D-64289 Darmstadt, Germany.

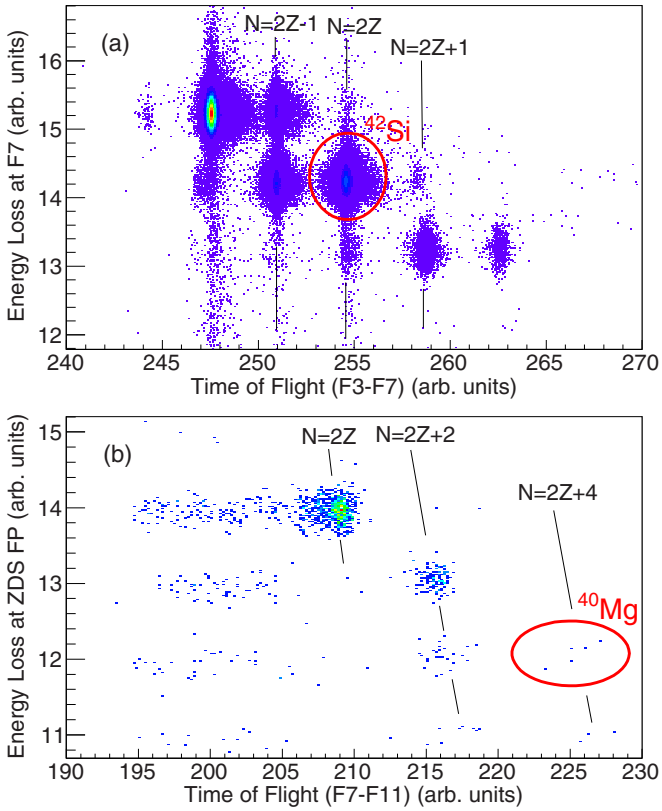

FIG. 1. (Color online) Particle identification plots for the (a) incoming ^{42}Si beam in BigRIPS and the (b) reaction products detected in the ZDS following reaction of the ^{42}Si beam on a 4.02 g/cm^2 C target. The BigRIPS separator was set for transmission of the ^{42}Si secondary beam, while the ZDS was set to optimize transmission of ^{40}Mg.

corrections for reactions induced on timing scintillators, for survival through the thick secondary target, and for transmission of fragments through the BigRIPS and ZDS separators, which was simulated in LISE++ [7] and verified by comparison of the simulated and experimental transmission of unreacted ^{42}Si. Unreacted beam was simulated in LISE++ to be transmitted through the ZDS with an efficiency of 62%, which agreed within 1% with the experimental data; the ^{40}Mg reaction products were simulated to be transported with a 60% transmission, with a conservative error of 5%.

Two-proton knockout, such as that from ^{42}Si to ^{40}Mg, is expected [8] to proceed as a direct reaction. The cross section for this process will depend on the structure (overlap) of the initial ^{42}Si ground state and final ^{40}Mg states and can be used to extract information on the structure of ^{40}Mg. A formalism to calculate cross sections for sudden, direct, two-nucleon removal reactions has been presented in Refs. [9–11]. The calculation combines eikonal reaction theory with shell-model structure information in the form of two-nucleon amplitudes (TNAs) describing the overlap between initial and final states. Test-case measurements [10,11] have confirmed the sensitivity of two-nucleon knockout reactions to the initial and final states and this approach has been applied to derive structure information; see, for example, Refs. [12,13].

TABLE I. Theoretical and experimental cross-sections for two-proton removal from ^{42}Si. Shell-model calculations for the two-nucleon amplitudes used the SDPFU-Si and SDPF-MU effective interactions. The reaction theory included both absorption and diffractive contributions to the cross-section. A factor $R_s(2N) = 0.5$ has been applied to the calculated values; see text for details.

State	Energy (MeV)	σ_{theor} (μb)	Energy (MeV)	σ_{theor} (μb)	σ_{exp} (μb)
Interaction	SDPF-MU		SDPFU-Si		
0^+	0	51	0	17	
2_1^+	0.732	16	0.546	4	
0_2^+	1.683	78	2.073	136	
Inclusive		145		157	40^{+27}_{-17}

In the present analysis, shell model TNAs connecting states in ^{42}Si and ^{40}Mg were calculated using the recently proposed SDPF-MU effective interaction [14]. The interaction is well tested in the region of neutron-rich nuclei below ^{48}Ca, reproducing 2_1^+ and 4_1^+ energies, as well as $B(E2)$ values in the S and Si isotopes approaching $N = 28$ [15]. However, before cross sections calculated using these TNAs can be compared with experiment, a renormalization in the form of an empirical two-nucleon suppression factor $R_s(2N) \times \sigma_{th}$ is required [10]. A value of $R_s(2N) = 0.5$ has been determined in spherical sd-shell nuclei, which are well described by the shell model and is consistent with two-nucleon removal in the region surrounding ^{40}Mg, in particular the two-proton removal from ^{44}S to ^{42}Si [15].

Calculated final-state $2p$-removal cross sections based on the SDPF-MU effective interaction, and including the suppression factor, are shown in the third column of Table I. The experimental inclusive cross-section value is significantly smaller than that predicted by theory, which includes a second 0^+ state in ^{40}Mg at an excitation energy of 1.683 MeV. Given the uncertainty in the ^{40}Mg neutron separation energy $S_n = 1.740(790)$ MeV reported in the 2012 Atomic Mass Evaluation [16] it is certainly plausible that this second 0_2^+ state lies above the one neutron threshold. In this case, only the ground-state 0_1^+ and the 2_1^+ are bound, the calculated inclusive cross-section becomes 67 μb, in better agreement with the measured value. The comparison with shell-model plus eikonal reaction theory calculations indicates that only one of the two predicted low-lying 0^+ states in ^{40}Mg is bound.

A similar cross-section analysis, using TNAs calculated with the SDPFU-Si effective interaction [3], tuned for $Z \leqslant 14$, was also performed (fifth column of Table I). While there are differences in the partitioning of cross section to individual states, both interactions yield the same conclusion when compared to data, namely that the experimental $2p$-removal cross section is consistent only with one 0^+ state in ^{40}Mg being bound.

The magnitude of the experimental ^{42}Si$(-2p)$ knockout cross section provides information regarding the number of bound states in ^{40}Mg. We show that one can use cross-section ratios along the $N = 28$ chain to further address the nature of the ground state in ^{40}Mg in terms of deformation or shape.

Before doing so it is instructive to briefly consider the ground-state properties of the $N = 28$ isotones.

The $N = 28$ shell closure is large at $Z = 20$ and low-lying states in ^{48}Ca are well described within a spherical shell model. However, below $Z = 20$, the size of the $N = 28$ shell gap is reduced as protons are removed from the $d_{3/2}$ orbital and there is an evolution of nucleon configurations and nuclear shape along the isotonic chain. Removing $d_{3/2}$ protons simultaneously reduces the effect of the repulsive $\pi d_{3/2}$-$\nu f_{5/2}$ and attractive $\pi d_{3/2}$-$\nu f_{7/2}$ interactions, which effectively pushes the two neutron f shells closer in energy [17]. At the same time, at $N = 28$ the spacing between the proton $\pi d_{5/2}$, $\pi s_{1/2}$, and $\pi d_{3/2}$ orbitals is narrowed [14,18–20]. With the narrowing of the $N = 28$ gap and the proton single-particle spacings, quadrupole excitations develop between the $\Delta l = 2$ $\nu p_{3/2}$ and $\nu f_{7/2}$ neutron orbitals and the $\pi d_{5/2}$ and $\pi s_{1/2}$ proton orbitals, resulting in well-deformed nuclear shapes.

A schematic understanding of the evolution of the shapes along the $N = 28$ isotones has been proposed [14] in terms of the quadrupole force driving mixing between $m = \pm 1/2$ substates in the near-degenerate proton $s_{1/2}$ and $d_{5/2}$ (or $d_{3/2}$) orbitals and changing the occupancy of the *prolate-driving* $l = 2, m = \pm 1/2$ substates [14]. For $^{44}_{16}$S, data and calculations [21–27] indicate well-developed prolate deformation in the ground state, accompanied by a coexisting spherical 0^+_2 excited state. This is understood given the increased occupancy of the $\pi d_{3/2}$, $m = \pm 1/2$ substates that occurs with the mixing, resulting in a proton configuration favoring prolate deformation. For ^{42}Si, at $Z = 14$, mixing reduces occupancy of the $d_{5/2}$, $m = \pm 1/2$ substate, favoring oblate deformation. One-proton and two-proton knockout reactions [13] support this schematic picture, and the prediction of large-scale shell-model calculations, such as those of Ref. [3], which predict an oblate ^{42}Si$_{28}$ ground state and prolate 0^+_2 excited state. At $Z = 12$, the schematic picture is less clear, as protons alone do not strongly favor prolate over oblate configurations, with the partially filled $d_{5/2}$ orbital providing more freedom in the available proton configurations. However, shell-model calculations [3] as well as mean-field calculations [28] predict a reversal of states in ^{40}Mg$_{28}$ as compared to ^{42}Si, back to a prolate ground state with a low-lying oblate 0^+_2 state.

The fact that data and calculations consistently indicate the low-energy structure in ^{44}S, ^{42}Si, and ^{40}Mg is dominated by two major co-existing configurations (spherical and prolate in ^{44}S, oblate and prolate in ^{42}Si and ^{40}Mg) suggests that a two-state(shape) mixing model can provide a useful description of their structure. Force *et al.* [22] used such a model to describe the low-energy structure of ^{44}S, while Fortune [29] applied a similar analysis to the (t, p) transfer reactions populating ^{32}Mg. Here, in the same manner as Fortune, we use a two-state mixing model applied to two-proton knockout reactions, to explore the evolution of the dominant low-energy nuclear configurations (shapes) along the $N = 28$ isotonic chain.

Beginning at ^{44}S, the ground-state wave function is assumed to be a spherical (S) and prolate (P) admixture, $|^{44}S, 0^+_1\rangle = 0.35\,|0^+;\mathrm{S}\rangle + 0.94\,|0^+;\mathrm{P}\rangle$, as given by Force *et al.* [22]. The S- and P-component amplitudes are determined by the ratio of the measured $B(E2)$ values connecting the 2^+_1 state and the first two 0^+ states. In ^{42}Si and ^{40}Mg we expect prolate (P) and oblate (O) deformed components to be the dominant low-energy configurations. We write their ground-state wave functions and those of the ^{42}Si(0^+_2) excited state as

$$|^{42}\mathrm{Si}, 0^+_1\rangle = +\alpha\,|0^+;\mathrm{O}\rangle + \beta\,|0^+;\mathrm{P}\rangle, \tag{1}$$

$$|^{42}\mathrm{Si}, 0^+_2\rangle = -\beta\,|0^+;\mathrm{O}\rangle + \alpha\,|0^+;\mathrm{P}\rangle, \tag{2}$$

$$|^{40}\mathrm{Mg}, 0^+_1\rangle = +\gamma\,|0^+;\mathrm{O}\rangle + \delta\,|0^+;\mathrm{P}\rangle. \tag{3}$$

Given these (and the ^{44}S ground-state) wave functions, the TNAs describing the initial to final state overlaps, $\langle A; f|A+2; i\rangle$, for the ^{44}S$(-2p)$ and ^{42}Si$(-2p)$ reactions are

$$T_{44\to42}(0^+_1) = 0.35(\alpha T_{\mathrm{SO}} + \beta T_{\mathrm{SP}}) + 0.94(\alpha T_{\mathrm{PO}} + \beta T_{\mathrm{PP}}), \tag{4}$$

$$T_{44\to42}(0^+_2) = 0.35(\alpha T_{\mathrm{SP}} - \beta T_{\mathrm{SO}}) + 0.94(\alpha T_{\mathrm{PP}} - \beta T_{\mathrm{PO}}), \tag{5}$$

$$T_{42\to40}(0^+_1) = \alpha(\delta T_{\mathrm{OP}} + \gamma T_{\mathrm{OO}}) + \beta(\delta T_{\mathrm{PP}} + \gamma T_{\mathrm{PO}}), \tag{6}$$

where the T_{XY} are the TNAs derived from the overlaps, $\langle A; \mathrm{Y}|A+2; \mathrm{X}\rangle$, of each initial (X) and final (Y) shape configuration, being either S, O, or P.

These individual TNAs, T_{XY}, involving initial and final configurations with different deformation, are calculated within the Nilsson and BCS framework using the methodology of Takemasa [30]. The wave functions are constructed by projection of the Nilsson and BCS wave functions onto a definite angular momentum state. Standard Nilsson spin-orbit and L^2 term strength parameters, $\kappa = 0.05$ and $\mu = 0.45$, were used for both neutrons and protons. The (quadrupole) deformations assumed are discussed below. The BCS calculation inputs (with nn and pp pairing only) used proton and neutron gap parameters Δ_p and Δ_n derived from the N, Z, and $(N - Z)/A$-dependent parameterization of Madland and Nix [31]. The weighted linear combinations of these T_{XY}, shown in Eqs. (4)–(6), then provide the structural input to the eikonal, two-proton removal cross-section calculations; for details see, e.g., Refs. [9] and [10].

Calculations were performed for initial- and final-state (quadrupole) deformations of $|\beta_2| = 0.25$, 0.35, and 0.4 for ^{44}S, ^{42}Si, and ^{40}Mg, respectively, consistent with available data [22] and theoretical calculations [3,32]. We consider what constraints, on the O- and P-component amplitudes in Eqs. (1)–(3), follow from the ^{42}Si$(-2p)$ cross-section measurement of this work in combination with recent ^{44}S$(-2p)$ data [33].

To do so, and guided by the currently available experimental information, we compare the ratio of measured cross sections to the following final states,

$$\mathcal{R} = [\sigma_{44\to42}(0^+_1) + \sigma_{44\to42}(0^+_2)]/\sigma_{42\to40}(0^+_1), \tag{7}$$

with that calculated using the model TNAs of Eqs. (4)–(6). The measured inclusive cross section for the ^{44}S$(-2p)$ reaction is 155(22) μb, with 55(8) μb identified as directly populating the 2^+_1 and proposed 4^+_1 states [33]. As this data set did not identify the 0^+_2 state, we assume that $[\sigma_{44\to42}(0^+_1) + \sigma_{44\to42}(0^+_2)]$ is thus 100(23) μb. An upper limit for $\sigma_{42\to40}(0^+_1)$ is given by

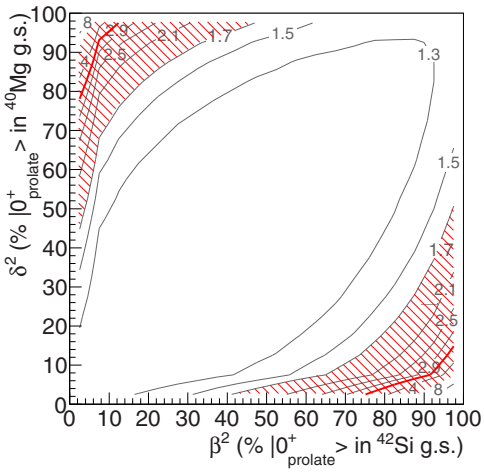

FIG. 2. (Color online) Percentage probabilities of the prolate (P) contributions in the ^{42}Si and ^{40}Mg ground-state wave functions, plotted as $\mathcal{P}_P(40) = \delta^2$ vs $\mathcal{P}_P(42) = \beta^2$. Contours correspond to specific values of cross-section ratios as labeled. Highlighted is the contour consistent with the empirical cross-section ratio limit of $\mathcal{R} \geqslant 1.7$ of Eq. (7). The solid red contour corresponds to the one-σ lower limit for $\mathcal{R}$, under the assumption that there is 25% feeding to the 2_1^+ state in the ^{42}Si(-2p) reaction.

our measured inclusive ^{42}Si($-2p$) cross section, of 40^{+27}_{-17} μb, giving an empirical value of $\mathcal{R} = 2.5^{+1.8}_{-1.2}$, or a one-$\sigma$ lower limit of $\mathcal{R} \geqslant 1.3$, assuming 100% of the cross section populates the ground state in the ^{42}Si $\rightarrow$ ^{40}Mg reaction.

However, it is worth noting that values of $\mathcal{R} > 1.3$ are *physically* more likely, due to some fraction of the observed inclusive ^{42}Si($-2p$) cross section feeding directly the ^{40}Mg(2_1^+) state. Assuming a branch to the 2^+ state of 25%, consistent with the SDPF-MU calculations, the calculated ratio becomes $\mathcal{R} = 3.3^{+2.4}_{-1.6}$. We consider the constraints this ratio puts on the O- and P-component amplitudes in Eqs. (1)–(3).

Figure 2 summarizes the full, correlated two-proton-removal cross-section results calculated for different O- and P-component amplitudes in ^{42}Si and ^{40}Mg. We present those percentage probabilities of the prolate (P) components, $\mathcal{P}_P(42) = \beta^2$ and $\mathcal{P}_P(40) = \delta^2$, in the ground-state wave functions, with gray contours corresponding to discrete values of $\mathcal{R}$, and the $\mathcal{R} = 3.3^{+2.4}_{-1.6}$ ratio value highlighted by the solid red contour and shaded region. While without further information, such as exclusive $\sigma_{44\rightarrow42}(0_1^+)$ and/or $\sigma_{44\rightarrow42}(0_2^+)$ measurements, we cannot uniquely constrain the predominant shapes of these ground states, it is clear from Fig. 2 that, from this analysis with $\mathcal{R} \geqslant 1.3$, ^{42}Si and ^{40}Mg are expected to be dominated by different ground-state configurations. The two-state mixing model calculations suggest that for a P-dominated ^{42}Si ground state, ^{40}Mg is likely to have only a small P-component in its ground state, or vice versa. That is, the dominant deformations in the ^{42}Si and ^{40}Mg ground states are consistently opposite in sign, and there are no solutions representing strongly mixed ground-state wave functions for both nuclei.

For a ^{42}Si ground state dominated by oblate deformation, as predicted in shell-model calculations [3] and supported by the schematic explanation of shapes provided in the analysis of Utsuno [14], then the two-state analysis predicts ^{40}Mg will have a dominantly prolate deformation. The change in the dominant ground-state configuration becomes more clear with larger cross-section ratios, $\mathcal{R}$.

In summary, the two-proton knockout reaction from ^{42}Si to ^{40}Mg has been studied at the RIBF at RIKEN. Using the high-intensity ^{48}Ca primary beam, the first direct reaction populating the heaviest known Mg isotope was observed with an inclusive cross section of 40^{+27}_{-17} μb. Comparison with calculations using shell-model structure inputs to eikonal model calculations indicates that only one of the two predicted low-lying 0^+ states in ^{40}Mg is bound. Further, the agreement with shell-model calculations using well-bound wave functions suggests that weak-binding effects are not yet manifesting in the ground-state structure of ^{40}Mg. Further analysis, using a two-state (shape) mixing model, suggests a change in the dominant components of the ground-state wave functions between ^{42}Si and ^{40}Mg. A consistent picture thus emerges, indicating a change in dominant nuclear shape from prolate in ^{44}S, to oblate in ^{42}Si, and returning to prolate in ^{40}Mg. This picture is consistent also with the deformation along the Mg isotopic chain, confirmed to ^{38}Mg by Doornenbal *et al.* [4] and anticipated to continue with well-developed prolate deformation in ^{40}Mg.

While the current cross-section measurement has provided first structural insight into ^{40}Mg, it is clear that additional spectroscopic information is needed to fully understand the structural evolution in this region. Identification of the 2_1^+ state in ^{40}Mg will provide an important test of theories of dripline nuclei and a benchmark for shell-model effective interactions applied in this challenging region of the nuclear chart.

This work was supported by the U.S. Department of Energy under Contract No. DE-AC02-05CH11231 (LBNL) and the JUSEIPEN program, and (for J.A.T.) by the United Kingdom Science and Technology Facilities Council (STFC) Research Grant No. ST/J000051. We thank the accelerator operations staff at RIBF/RIKEN Nishina Center for their work in primary beam delivery and the BigRIPS team for preparing the secondary beam.

[1] T. Baumann *et al.*, Nature (London) **449**, 1022 (2007).
[2] O. Sorlin and M-G. Porquet, Phys. Scr. T **152**, 014003 (2013).
[3] F. Nowacki and A. Poves, Phys. Rev. C **79**, 014310 (2009).
[4] P. Doornenbal *et al.*, Phys. Rev. Lett. **111**, 212502 (2013).
[5] T. Kubo, Nucl. Instrum. Methods Phys. Res. B **204**, 97 (2003).
[6] Y. Mizoi, T. Kubo, H. Sakurai, K. Kusaka, K. Yoshida, and A. Yoshida, RIKEN Accel. Prog. Rep. **38**, 297 (2005).
[7] O. B. Tarasov and D. Bazin, Nucl. Instrum. Methods Phys. Res. B **266**, 4657 (2008).
[8] D. Bazin *et al.*, Phys. Rev. Lett. **91**, 012501 (2003).

[9] J. A. Tostevin, G. Podolyak, B. A. Brown, and P. G. Hansen, Phys. Rev. C **70**, 064602 (2004).
[10] J. A. Tostevin and B. A. Brown, Phys. Rev. C **74**, 064604 (2006).
[11] K. Yoneda *et al.*, Phys. Rev. C **74**, 021303(R) (2006).
[12] P. Fallon *et al.*, Phys. Rev. C **81**, 041302(R) (2010).
[13] S. Takeuchi *et al.*, Phys. Rev. Lett. **109**, 182501 (2012).
[14] Y. Utsuno, T. Otsuka, B. A. Brown, M. Honma, T. Mizusaki, and N. Shimizu, Phys. Rev. C **86**, 051301(R) (2012).
[15] J. A. Tostevin, B. A. Brown, and E. C. Simpson, Phys. Rev. C **87**, 027601 (2013).
[16] M. Wang, G. Audi, A. H. Wapstra, F. G. Kondev, M. MacCormick, X. Xu, and B. Pfeiffer, Chin. Phys. C **36**, 1603 (2012).
[17] L. Gaudefroy *et al.*, Phys. Rev. Lett. **97**, 092501 (2006).
[18] A. Gade *et al.*, Phys. Rev. C **74**, 034322 (2006).
[19] L. Riley *et al.*, Phys. Rev. C **78**, 011303 (2008).
[20] O. Sorlin and M.-G. Porquet, Prog. Part. Nucl. Phys. **61**, 602 (2008), and references therein.
[21] S. Grévy *et al.*, Eur. Phys. J. A **25**, 111 (2005).
[22] C. Force *et al.*, Phys. Rev. Lett. **105**, 102501 (2010).
[23] J. Fridmann *et al.*, Nature (London) **435**, 922 (2005).
[24] J. Fridmann *et al.*, Phys. Rev. C **74**, 034313 (2006).
[25] B. Bastin *et al.*, Phys. Rev. Lett. **99**, 022503 (2007).
[26] D. Santiago-Gonzalez *et al.*, Phys. Rev. C **83**, 061305(R) (2011).
[27] L. Cáceres *et al.*, Phys. Rev. C **85**, 024311 (2012).
[28] R. Rodríguez-Guzmán, J. L. Egido, and L. M. Robledo, Phys. Rev. C **65**, 024304 (2002).
[29] H. T. Fortune, Phys. Rev. C **84**, 024327 (2011).
[30] T. Takemasa, Comput. Phys. Commun. **36**, 79 (1985).
[31] D. G. Madland and J. R. Nix, Nucl. Phys. A **476**, 1 (1988).
[32] Z. P. Li, J. M. Yao, D. Vretenar, T. Niksić, H. Chen, and J. Meng, Phys. Rev. C **84**, 054304 (2011).
[33] M. Matsushita and S. Takeuchi (private communication).